PNAS RESEARCH ARTICLE | PHYSIOLOGY OPEN ACCESS

Brain dysfunction during warming is linked to oxygen limitation in larval zebrafish

Anna H. Andreassen[a], Petter Hall[a], Pouya Khatibzadeh[a], Fredrik Jutfelt[a,b], and Florence Kermen[a,c,1]

Edited by George Somero, Stanford University, Pacific Grove, CA; received April 23, 2022; accepted August 9, 2022

Understanding the physiological mechanisms that limit animal thermal tolerance is crucial in predicting how animals will respond to increasingly severe heat waves. Despite their importance for understanding climate change impacts, these mechanisms underlying the upper thermal tolerance limits of animals are largely unknown. It has been hypothesized that the upper thermal tolerance in fish is limited by the thermal tolerance of the brain and is ultimately caused by a global brain depolarization. In this study, we developed methods for measuring the upper thermal limit (CT_{max}) in larval zebrafish (*Danio rerio*) with simultaneous recordings of brain activity using GCaMP6s calcium imaging in both free-swimming and agar-embedded fish. We discovered that during warming, CT_{max} precedes, and is therefore not caused by, a global brain depolarization. Instead, the CT_{max} coincides with a decline in spontaneous neural activity and a loss of neural response to visual stimuli. By manipulating water oxygen levels both up and down, we found that oxygen availability during heating affects locomotor-related neural activity, the neural response to visual stimuli, and CT_{max}. Our results suggest that the mechanism limiting the upper thermal tolerance in zebrafish larvae is insufficient oxygen availability causing impaired brain function.

heat stress | spreading depolarization | CT_{max} | thermal limit | calcium imaging

Heat waves are becoming more frequent and severe as climate change progresses (1, 2). Ectothermic animals might be particularly vulnerable to extreme heat, as their biological rates are directly affected by the ambient temperature (3–5). The range of temperatures an ectotherm can tolerate is bounded at the upper end by an upper thermal limit. During gradual heating, the critical thermal maximum (CT_{max}), that is, the temperature at which their locomotor function is lost and their movement becomes disorganized, is commonly used to describe the upper thermal limit (6–8). The thermal tolerance limits of aquatic ectotherms correlate with the water temperature in geographical distributions (9), suggesting that limits in thermal tolerance partly determine distribution ranges. Furthermore, rapid water warming during heat waves can cause mass mortality in fishes (10). Knowledge of the physiological dysfunction that limits thermal tolerance is therefore an important part of understanding how ectotherms may respond to increasingly warmer temperatures and in predicting ecosystem impacts. Several hypotheses about the limitations of thermal tolerance have been proposed, but the causes of thermal limits remain debated (11–14).

Oxygen limitations have long been a focus in studies of thermal tolerance (15). The oxygen- and capacity-limited thermal tolerance (OCLTT) hypothesis suggests that the cardiorespiratory system in ectotherms is unable to compensate for the temperature-induced increase in oxygen requirement, leading to tissue hypoxia and thus setting the limits for thermal tolerance (16–18). A mismatch between oxygen delivery and the increasing oxygen demand at high temperatures or near upper thermal limits has been reported in invertebrates and fishes (19–22), while sufficient cardiorespiratory supply of oxygen is maintained in a number of other ectotherms (23, 24). In addition, experimental manipulation of oxygen availability during heat stress often fails to affect thermal tolerance (25). These contrasting results from a considerable amount of literature suggest that the OCLTT hypothesis can only partly explain thermal tolerance limits and that these oxygen effects on thermal tolerance is species and context dependent (12, 18, 24, 26, 27). Finally, the OCLTT hypothesis does not specify which physiological or cellular mechanisms fail as a result of insufficient oxygen supply (26).

Another major hypothesis about limits of upper thermal tolerance is based on temperature-induced neural dysfunction (28). Neural control of locomotion is a heat-sensitive physiological mechanism that may become disrupted at high temperatures and lead to impaired locomotion at CT_{max}. Temperature-induced neural dysfunction (i.e., altered neural activity) could consequently underlie upper thermal tolerance limits, either via direct thermal effects on neurons (11, 12) or via indirect thermal effects from oxygen limitation (20). Examples of severe heat-induced neural dysfunctions include spreading

Significance

Aquatic organisms face lethal temperatures during the increasingly frequent heat waves. Knowledge of what limits survival in extreme temperatures is thus critical to predict how organisms will respond to climate change. We measured neural activity in larval fish during warming at different oxygen levels to test whether brain activity limited thermal tolerance, and whether oxygen affected the thermal limit. Brain activity was reduced when the thermal limit was reached and was followed by a global depolarization in the brain. Oxygen concentration affected spontaneous neural activity, neural responsiveness to stimuli, and thermal tolerance. These results reveal that neural activity is suppressed before the thermal limit is reached and that acute warming tolerance is limited by oxygen levels in a tropical fish.

Author affiliations: [a]Department of Biology, Faculty of Natural Sciences, Norwegian University of Science and Technology, Trondheim, 7491 Norway; [b]Department of Biological and Environmental Sciences, Faculty of Science, University of Gothenburg, Gothenburg, 405 30 Sweden; and [c]Department of Neuroscience, Faculty of Health and Medical Sciences, University of Copenhagen, 2200 Copenhagen, Denmark

Author contributions: A.H.A., P.H., F.J., and F.K. designed research; A.H.A., P.H., and P.K. performed research; F.J. contributed new reagents/analytic tools; A.H.A., P.H., and F.K. analyzed data; and A.H.A. and F.K. wrote the paper.

The authors declare no competing interest.

This article is a PNAS Direct Submission.

[1]To whom correspondence may be addressed. Email: florence.kermen@sund.ku.dk.

This article contains supporting information online at http://www.pnas.org/lookup/suppl/doi:10.1073/pnas.2207052119/-/DCSupplemental.

Published September 19, 2022.

depolarizations in the brain of fruit flies (29), loss of rhythmic neural activity in the digestive system of the Jonah crab (30), and thermogenic seizures in vertebrates (31–33). However, few studies have directly investigated how neural dysfunction relates to measurements of thermal tolerance. In fruit flies, spreading depolarizations measured in restrained flies occur at similar temperatures as a heat-induced coma in freely moving conspecifics (29). Similarly, local heating of the cerebellum caused goldfish to lose equilibrium at similar temperatures as during warming of the whole animal (11), and a study on Atlantic cod found that cooling the brain marginally increased CT_{max}, suggesting a causal link between brain function and thermal tolerance (12). It has also been shown that the electrical properties of brain and myocardial cells are affected by heat, potentially causing the failure of multiple tissues at high temperatures (14).

The relative importance of direct thermal effects on neural function and oxygen effects has been subject to considerable discussion in the literature on thermal limits (12, 26, 34–36). The investigation of thermal limits in neural function has been hindered by technical challenges. For example, it has not been possible to record brain activity and measure CT_{max} simultaneously during acute warming in freely moving animals.

In this study, we solved that challenge through a series of five heat-ramping experiments on transparent larval zebrafish (*Danio rerio*) expressing a genetically encoded calcium indicator in neurons throughout the brain (37). This allowed simultaneous recording of neural activity, CT_{max}, and cardiac activity, and allowed us to study effects of oxygen availability during heat ramping. We tested three main predictions: 1) if neural dysfunction in the brain limits thermal tolerance, a neural dysfunction should coincide with, CT_{max}; 2) a seizure or global spreading depolarization is the neural mechanism that causes CT_{max}; 3) neural dysfunction is caused by oxygen limitation, and water oxygen manipulation similarly affects both neural function and CT_{max}.

RESULTS

CT_{max} Is Similar in Larval and Adult Zebrafish. In experiment 1, we established a protocol for measuring CT_{max} in 5-d-old zebrafish larvae. Activity was recorded in freely swimming larvae in a custom-designed glass heating mantle placed under a camera (Fig. 1 *A* and *B*). The larvae were either exposed to a water temperature increasing from 28 °C at a rate of 0.3 °C/min (hereafter, "heat-ramp fish"; $n = 12$) or maintained at 28 °C (control fish, $n = 14$).

To establish a protocol for measuring larval CT_{max}, we examined how the following activity measures were affected during heat ramping compared with control trials: swimming speed (*SI Appendix*, Fig. S1*A*), spiral swimming (*SI Appendix*, Fig. S1 *B* and *C* and Movie S1), loss of equilibrium (*SI Appendix*, Fig. S1 *C* and *D* and Movie S2), and loss of response (i.e., no escape to repeated touches to the trunk) (*SI Appendix*, Fig. S1*E* and *Methods*). There was no difference in swimming speed between control and heat-ramp fish throughout the assay (*SI Appendix*, Table S1). Spiral swimming, loss of equilibrium and loss of response occurred toward the end of the assay in heat-ramp fish (*SI Appendix*, Fig. S1*C*) and were significantly more prevalent than in control fish (*SI Appendix*, Fig. S1*B*, *D* and *E* and Tables S2 and S3). Yet, spiral swimming was not systematically observed in heat-ramp fish, and loss of equilibrium was relatively unspecific, as it also occurred in control fish held at normal temperature. On the other hand, all heat-ramp fish eventually became unresponsive to repeated trunk stimulation (loss of response), and all control fish maintained a functional escape response throughout the assay (*SI Appendix*, Fig. S1*E*). We concluded that loss of response was a systematic and specific measure of loss of function during warming and therefore a suitable end point for determining larval CT_{max}.

Using the loss of response as the end point for CT_{max}, we found that 5-d-old heat-ramp fish reached CT_{max} at 41.4 ± 0.1 °C (Fig. 1*C*). We repeated the experiment with 9-d-old fish ($n = 12$) and found that they reached CT_{max} at similar temperatures (41.3 ± 0.2 °C; 5 d postfertilization [dpf]: 9 dpf: $P = 0.7$ (*SI Appendix*, Table S3). This indicates that the loss-of-response criterion is stable during larval development (Fig. 1*C*). Furthermore, adult zebrafish ($n = 15$) tested using the loss-of-equilibrium protocol (8) reached CT_{max} at similar temperatures (41.0 ± 0.1 °C) as those of larvae (5 dpf: adult: $P = 0.07$; 9 dpf: adult: $P = 0.2$) (Fig. 1*C*).

Warming Causes Neural Dysfunctions Near the Upper Thermal Limit. Neurons operate best within a certain thermal range (30, 38, 39). Therefore, we hypothesized that neural dysfunction could explain the heat-induced locomotor impairments and loss of response that we observed at the upper thermal limit of the fish (Fig. 1*C* and *SI Appendix*, Fig. S1*E*). To measure neural

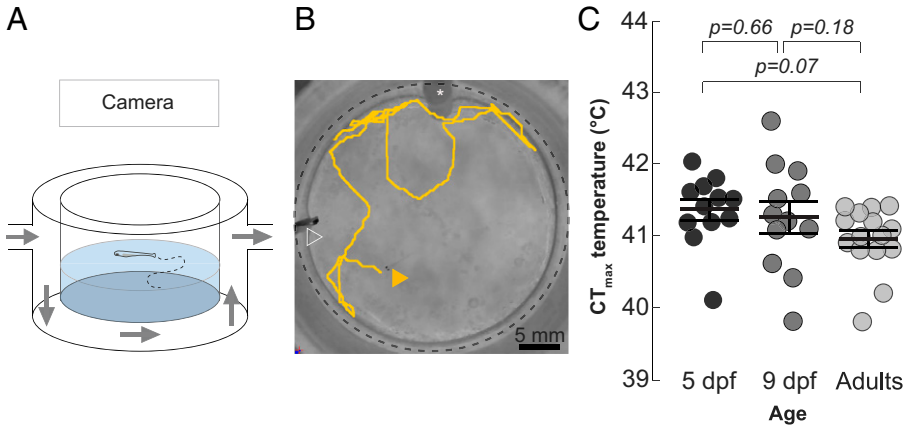

Fig. 1. The upper thermal limit in freely swimming zebrafish larvae and adults. (*A* and *B*) Schematic figure (*A*) and photo with top view (*B*) of the experimental setup for CT_{max} measurement in freely swimming zebrafish larvae. (*B*) Larva initial position is indicated by a yellow, filled arrowhead and the trajectory is represented in yellow during the following 30 s. The dashed black circle indicates the walls of the central chamber. The white arrowhead indicates the position of a thermocouple. The white asterisk indicates the tube for bubbling. (*C*) CT_{max} (temperature at loss of response for 5 and 9 d postfertilization [dpf] and loss of equilibrium for adults; see *Methods*) in 5-d-old ($n = 12$; black circles), 9-d-old ($n = 12$; dark gray circles), and adult fish ($n = 15$; light gray circles) (*SI Appendix*, Table S3). The bars and error bars indicate the group mean ± SE.

activity during heat ramping, 5-d-old larvae expressing the calcium indicator GCaMP6s in most neurons throughout the brain were mounted in agarose (restrained) in the heating mantle and placed under an epifluorescence microscope, in experiment 2 (Fig. 2 *A* and *B*).

Prominent neural activity could be observed in the medulla of both heat-ramp ($n = 11$) and control ($n = 8$) fish (Fig. 2 *C* and *D*), which was quantified by calculating the frequency of detected calcium peaks (Fig. 2*F*). These calcium peaks likely correspond to attempted tail beats, as reported in previous studies (40, 41). Medullar activity remained stable at 1.6 ± 0.1 peaks/min in the control fish (time: $P = 0.4$; time^2: $P = 0.3$) (Fig. 2 *C* and *F* and *SI Appendix*, Table S4). Conversely, in heat-ramp fish, the medullar activity more than doubled with temperature, and reached 3.6 ± 0.4 peaks/min prior to a sharp decline below control levels before a large seizure-like brain-wide depolarization occurred (time × heat ramp: $P < 0.001$; time^2 × heat ramp: $P < 0.001$) (Fig. 2 *D* and *F*, *SI Appendix*, Table S4). Plotting medullar activity across temperature confirmed this pattern (*SI Appendix*, Fig. S2*A*), with a strong decrease in medullar activity compared with the control, occurring at 39 to 41 °C.

During the massive depolarization in heat-ramp fish, the telencephalon and the medulla, which were otherwise weakly coactive (Fig. 2 *C* and *D*), both displayed a prominent increase in neural activity (Fig. 2*D*). The temporal aspect of the spreading depolarization is illustrated in a laterally mounted fish in Fig. 2*E* and Movie S3: it spread relatively slowly and reached the dorsal brain regions 10 to 12 s after the onset in the ventral diencephalon. The heat-induced, brain-wide depolarizations started at 40.5 ± 0.4 °C in agar-embedded fish (*Fig. 2*G), which is close to the CT_{max} temperature recorded in freely swimming, age-matched fish in experiment 1 (41.4 ± 0.1 °C) (Fig. 1*C*) Upon detection of the brain-wide depolarization, the water temperature was rapidly decreased to 28 °C and brain activity recovered 10 to 15 min after the brain-wide depolarization (Fig. 2*D*).

Together, the results of this second experiment show that several heat-induced neural dysfunctions occur near the upper thermal limit of zebrafish larvae. First, neural activity in locomotor brain centers is strongly reduced. Second, a substantial

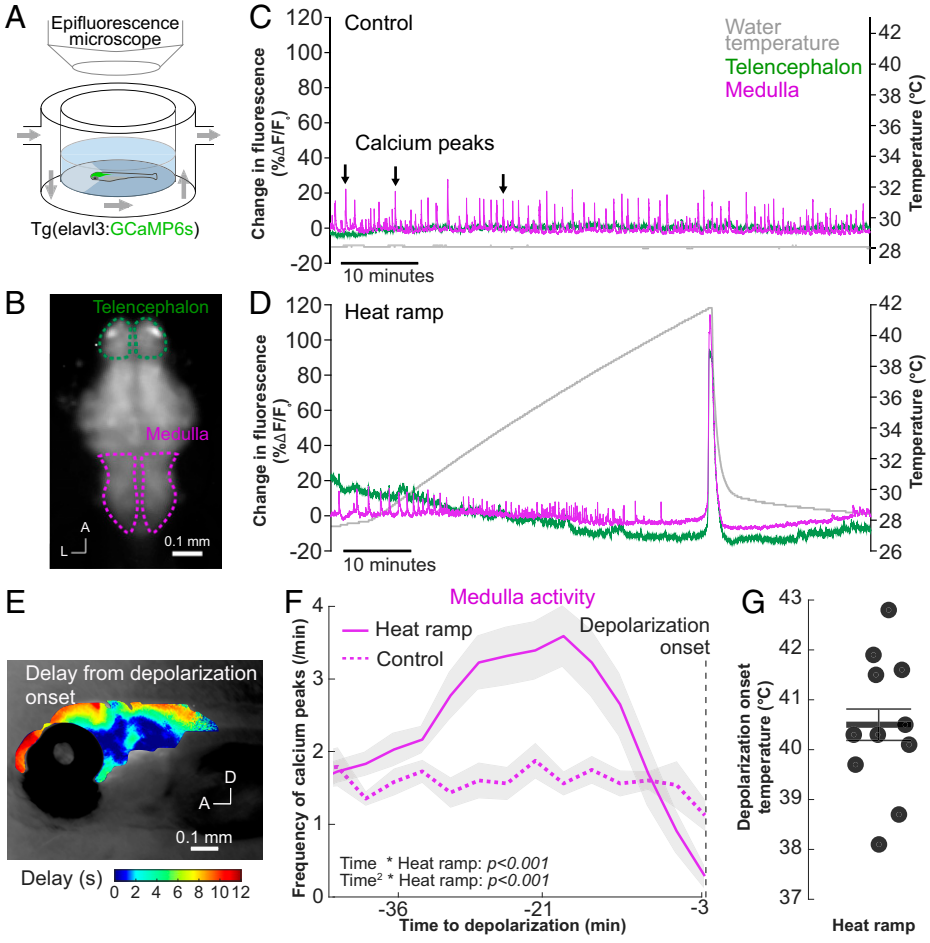

Fig. 2. Embedded zebrafish larvae develop brain-wide depolarizations near the upper thermal limit. (*A* and *B*) Schematic overview (*A*) and image (*B*) of the experimental setup for whole-brain neural activity measurement in agar-embedded, 5-d-old *Tg(elavl3:GCaMP6s)* zebrafish larva. (*B*) Raw fluorescence image of the larva brain highlighting the telencephalon (dashed green lines) and medulla (dashed magenta lines). A, anterior; L, lateral. (*C* and *D*) Change in fluorescence (% $\Delta F/F_0$; left *y*-axis) in the telencephalon and medulla of a representative control larva (*C*) and a representative heat-ramp larva (*D*). The water temperature (gray) was maintained at 28 °C throughout the recording (right *y*-axis in *C*) for the control fish and was increased during a heat-ramp treatment (0.3 °C/min) until a brain-wide depolarization was detected and then rapidly adjusted to 28 °C until the end of the recording (right *y*-axis in *D*). Note the return to holding temperature in heat-ramp fish and recovery of normal brain activity and calcium peaks 10 to 15 min after the brain-wide depolarization in *D*. (*E*) Heat map illustrating the temporal spread of the depolarization throughout the brain in a representative heat-ramp fish mounted laterally (*Methods*). D, dorsal. (*F*) Frequency of medulla calcium peaks in heat-ramp fish ($n = 11$; magenta line) during the 50 min preceding the brain-wide depolarization and during the corresponding period in control fish ($n = 8$; magenta dashed line) (*SI Appendix*, Table S4). The depolarization onset in heat-ramp fish is indicated by a dashed vertical line. (*G*) Temperature at depolarization onset in heat-ramp fish ($n = 11$). (*F* and *G*) Data are presented with mean (solid line) and SE (shaded area) in (*F*) and with a bar and error bars in (*G*).

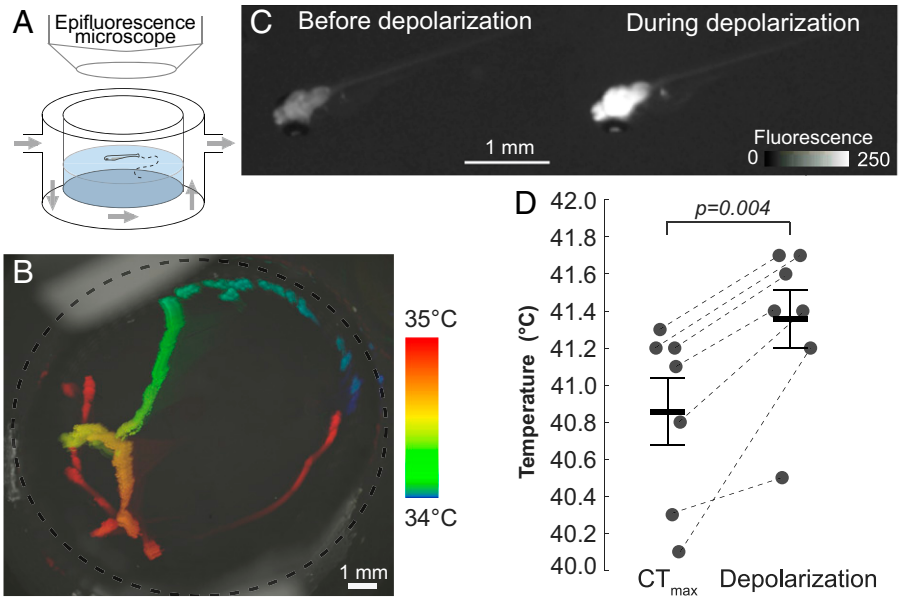

Fig. 3. CT_{max} precedes the brain-wide depolarization in freely swimming zebrafish larvae. (*A*) Schematic overview of the experimental setup for calcium imaging in freely swimming, 5-d-old *Tg(elavl3:GCaMP6s)* zebrafish larvae. (*B*) Top view of setup with color-coded time projection of a heat-ramp fish's movements in the setup for 3 min (34 to 35 °C). (*C*) Representative images of brain fluorescence in the same fish as in *B*, before (*Left*) and during (*Right*) the brain-wide depolarization. (*D*) CT_{max} and depolarization-onset temperatures measured in heat-ramp fish (black circles; $n = 7$) (*SI Appendix*, Table S5). The bars and error bars indicate the mean and SE.

wave of depolarization propagates throughout the brain at temperatures close to the upper thermal limit of freely swimming conspecifics.

CT_{max} Precedes the Brain-Wide Depolarization. To test whether a brain dysfunction (e.g., the observed global depolarization) limits thermal tolerance, we sought to establish the relative timing of CT_{max} and the heat-induced neural dysfunctions observed in experiment 2. To do so, we simultaneously measured CT_{max} and neural activity in freely swimming zebrafish during a heat ramp using epifluorescence imaging in experiment 3 (Fig. 3 *A* and *B*). CT_{max} (40.9 ± 0.2 °C) preceded the brain-wide depolarization (41.4 ± 0.2 °C) (Fig. 3*C*) in all individuals, by 0.5 °C on average ($P = 0.004$) (Fig. 3*D* and *SI Appendix*, Table S5). These results from freely swimming fish show that brain-wide depolarizations were not an artifact due to agarose embedding (Fig. 2). We concluded that CT_{max} is not preceded by the brain-wide depolarization but instead occurs during the period of reduced medulla activity.

Cardiac Function Is Reduced Prior to the Brain-Wide Depolarization. Next, we sought to test whether the activity of the heart, which contains excitable cells like the neural tissue, would also be altered at high temperatures. To test this hypothesis, we simultaneously measured neural activity and heart rate in larvae embedded laterally in experiment 4 (Fig. 4 *A* and *B*). The neural activity in the medulla displayed similar dynamics as in experiment 2, with an increase from 28 to 34 °C and a decrease at 37 °C (*SI Appendix*, Fig. S2*B*). The heart rate increased with a Q_{10} value (i.e., the rate of change with a 10 °C increase in temperature) of 1.5 (from 4.4 ± 0.1 Hz to 5.7 ± 0.1 Hz) between 28 and 34 °C ($P < 0.001$) (Fig. 4*C* and *SI Appendix*, Table S6). From 34 to 37 °C, the heart rate decreased ($Q_{10} = 0.6$) to 4.7 ± 0.2 Hz ($P < 0.001$), after which it remained stable in the period prior to the brain-wide depolarization ($P = 0.6$) (Fig. 4*C*). The heart rate also remained unchanged during the brain-wide depolarization (Fig. 4 *D* and *E*).

Altogether, no abrupt failure in cardiac activity (e.g., cardiac arrest) was detected during the period prior to the brain-wide depolarization, when CT_{max} occurs. Yet, after an initial increase in heart rate with temperature, the heart rate dropped under further heating. This could be due to similar mechanisms that cause the reduction in neural activity prior to CT_{max} (*SI Appendix*, Fig. S2). Furthermore, this decrease in heart rate before CT_{max} could result in insufficient oxygen and metabolic supply to tissues including the brain, if the cardiac function does not match the increased metabolic requirements at high temperatures.

Oxygen Availability Affects Neural Function and CT_{max}. In experiment 5, we tested the effect of oxygen availability on thermal tolerance by exposing freely swimming larvae to a water oxygen level of either 60% (hypoxic), 100% (normoxic), or 150% (hyperoxic) air-saturated water. CT_{max} occurred at 39.1 ± 0.1 °C in the hypoxia treatment ($n = 24$), 0.5 °C lower than in normoxia (39.6 ± 0.1 °C; $n = 28$; $P = 0.007$) (Fig. 5*A*, *SI Appendix*, Table S7). Conversely, CT_{max} occurred at 40.1 ± 0.2 °C in the hyperoxia treatment ($n = 21$), 0.5 °C higher than in normoxia ($P = 0.025$). This indicates that oxygen availability affects thermal tolerance in larval zebrafish.

To test the effect of oxygen availability on neural activity, we also applied the same treatments (60%, 100%, and 150% air-saturated water) to agar-embedded larvae placed under an epifluorescence microscope. The brain-wide depolarization occurred at 40.2 ± 0.3 °C in normoxia ($n = 12$) and occurred at 2.5 °C lower in hypoxia (37.7 ± 0.5 °C; $n = 14$; $P < 0.001$) (Fig. 5*B* and *SI Appendix*, Table S8). Conversely, the hyperoxia treatment ($n = 14$) increased the depolarization temperature by 1.3 °C compared with normoxia (41.5 ± 0.2 °C; $P = 0.003$). Oxygen level did not change the amplitude of the brain-wide depolarization (hypoxia: normoxia: $P = 0.3$; normoxia: hyperoxia: $P = 0.5$); however, the oxygen limitation significantly prolonged the recovery time after the depolarization (hypoxia: normoxia: $P < 0.001$; normoxia: hyperoxia: $P = 0.1$) (*SI Appendix*, Fig. S3 *A*–*C* and Table S8). These results indicate that oxygen availability strongly influences the onset of the heat-induced brain-wide depolarization in larval zebrafish.

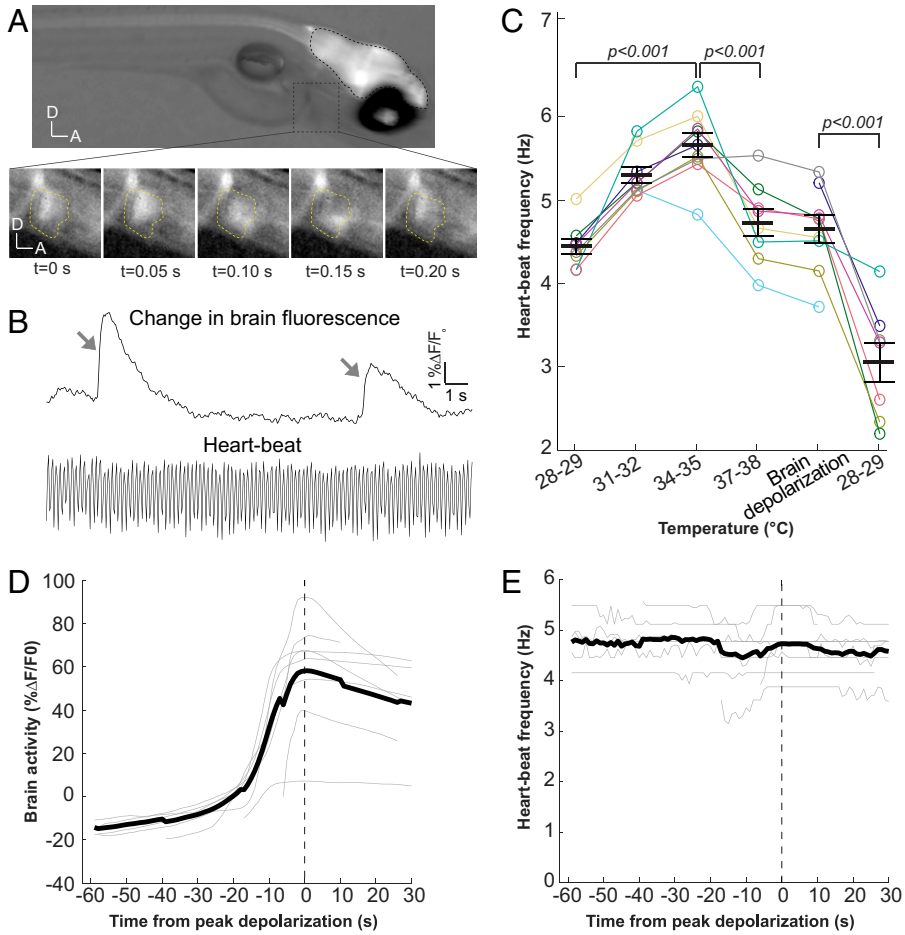

Fig. 4. Heart rate before and during the brain-wide depolarization in embedded zebrafish larvae. (*A, Top*) Representative example of simultaneous neural-activity and heart-rate imaging in a 5-d-old *Tg(elavl3:GCaMP6s)* zebrafish larva embedded laterally in agar, using epifluorescence microscopy. The brain is outlined with black dashed lines and the heart with a dashed gray square. (*Bottom*) The heart region (dashed yellow line) is shown in inverted greyscale (A, anterior; D, dorsal) during a cardiac cycle. (*B*; *Top*) Change in brain fluorescence (%$\Delta F/F_0$) in the same fish as in *A*, at 31 °C. Changes in brain fluorescence are indicated by gray arrows. (*Bottom*) Change in luminosity within a region of interest in the heart during the same period, which is used to calculate the heart rate. (*C*) Average heart rate in embedded heat-ramp fish (n = 9). The *x*-axis shows ranges of 1 °C elevation during which the heart rate was measured. The fifth temperature category (brain depolarization) corresponds to heart rate during the 60 s before and the 30 s after peak brain depolarization. The sixth category corresponds to heart rate after fish were rapidly returned to holding temperature. Horizontal bars and error bars indicate the mean and SE. The colored lines represent individual fish (*SI Appendix*, Table S6). (*D* and *E*) Change in neural activity (*D*) and heart rate (*E*) during the brain-wide depolarization (same period as brain depolarization in *C*). Gray lines represent individual fish and the thick black line represents the mean. All traces are aligned with respect to the peak fluorescence (vertical dashed line).

To further examine the effect of oxygen availability on neural activity, we compared the frequency of calcium peaks in the medulla (Fig. 5*C*) between the different oxygen treatments. In all groups, the medullar activity sharply decreased in the minutes prior to the brain-wide depolarization (*SI Appendix*, Fig. S3*D*), in line with our previous results (Fig. 2*F*). Neural activity in the medulla increased until 36 °C (Q_{10} = 1.8) in the normoxia treatment (n = 10), reaching a maximum frequency of 2.5 ± 0.4 peaks/min. The frequency of calcium peaks increased at a higher rate in the hyperoxia treatment (Q_{10} = 1.9; n = 11) and reached a higher maximum frequency of 3.3 ± 0.3 peaks/min at 37 °C. In the hypoxia treatment (n = 12), contrarily, the frequency decreased with temperature from the start of the trial at an accelerating rate (Q_{10} at 28 to 34 °C = 0.8; Q_{10} at 34 to 38 °C = 0.02) (Fig. 5*D* and *SI Appendix*, Table S9). This demonstrates that increased oxygen availability preserved neural activity in the locomotor center and that oxygen limitation reduced locomotor-related brain activity near the upper thermal limit of the fish larvae.

Decreased or increased oxygen availability during heat ramping resulted in depressed or improved neural activity in the medulla and decreased or increased thermal limits, respectively (Fig. 5). The results can be explained by a causal link between heat-impaired neural function and CT_{max}, whereby neural dysfunctions at the upper thermal limit culminates in the larvae's loss of response. An alternative explanation could be that neural function is preserved at high temperatures under low oxygen conditions, but that the decreased neural activity in locomotor centers instead results from less frequent swimming attempts.

To discriminate between those two mechanisms, and to test whether neural responsiveness is affected at high temperatures and covary with thermal limits, we measured light-evoked responses in the optic tectum of the same fish used in experiment 5 during heating (Figs. 5 *B* and 6 *A* and *B*). The amplitude of light-evoked responses decreased with increasing temperature in all treatments (*SI Appendix*, Fig. S4 *A* and *B*). To compensate for interindividual variation in the light-evoked neural activity, we categorized the individual response to the light flashes as *response* or *no response* (*Methods*, Fig. 6*C*, and *SI Appendix*, Fig. S4*C*). In normoxia (n = 11), the optic tectum responses were initially recorded to 31% of the light flashes until 31 °C, after which the responsiveness gradually decreased with further heating (Fig. 6*C*). In hypoxia (n = 14), the proportion of neural responses decreased from 33% from the start of the heat ramp. The hyperoxic treatment

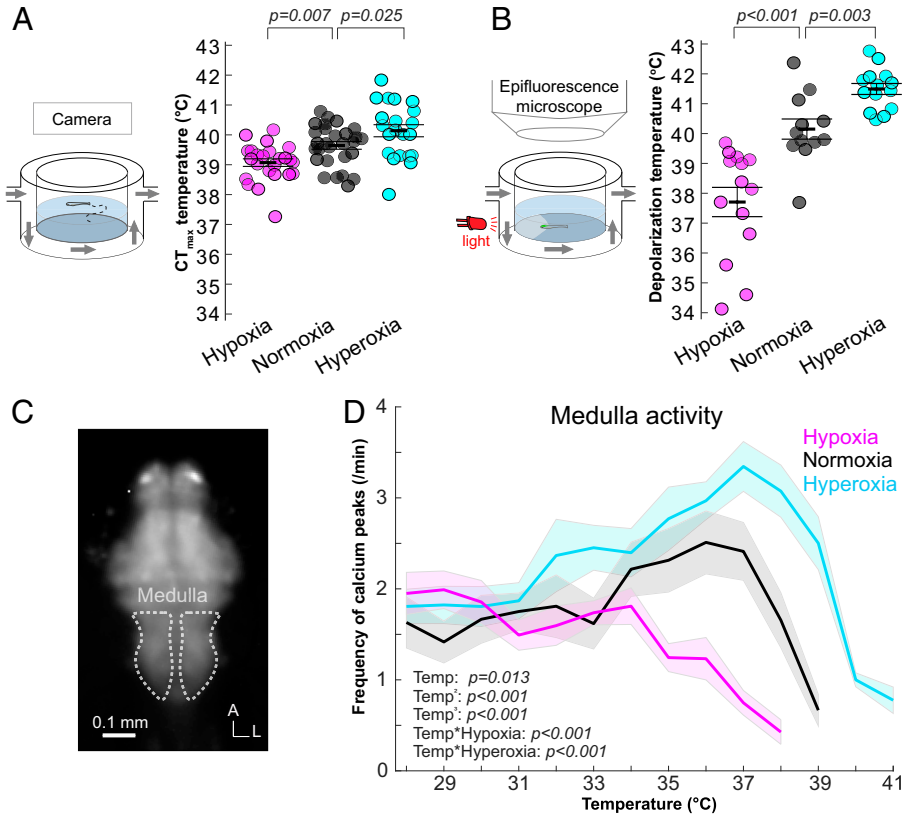

Fig. 5. Oxygen availability affects both CT_{max} and onsets of neural dysfunctions. (*A*) Effect of oxygen availability on CT_{max} measured in freely swimming fish (setup illustrated in *Left* panel) during heat ramping with water oxygen level of 60% (hypoxia; magenta circles; $n = 24$), 100% (normoxia; black circles; $n = 28$), or 150% (hyperoxia; cyan circles; $n = 21$) of air-saturated water (*SI Appendix*, Table S7). (*B*) Brain-wide depolarization-onset temperatures measured in agar-embedded, *Tg(elavl3:GCaMP6s)* 5-d-old fish (setup illustrated in *Left* panel) during heat ramping in hypoxia ($n = 14$), normoxia ($n = 12$), and hyperoxia ($n = 14$) (*SI Appendix*, Table S8). It is important to bear in mind that CT_{max} (*A*) and neural (*B*) data were collected in freely swimming versus embedded larvae, respectively, and that direct comparisons of these temperatures should be interpreted with caution. (*C*) Image outlining the medulla where the frequency of calcium peaks was measured. A, anterior; L, lateral. (*D*) Frequency of medulla calcium peaks during heat ramping in hypoxia ($n = 12$), normoxia ($n = 10$), and hyperoxia ($n = 11$) (*SI Appendix*, Table S9). (*A*, *B*, *D*). Results for hypoxia (60%; magenta), normoxia (100%; black), and hyperoxia (150%; cyan) are presented with mean and SE (*A* and *B*: bars and error bars; *D*: solid lines and shaded area). Temp, temperature.

($n = 13$) increased the resilience of sensory response to heating by 5 °C, as a responsiveness of 36% was maintained up to 36 °C before it decreased with further heating (*SI Appendix*, Table S10).

Altogether, these results show that normal neural function is reduced during heating before CT_{max}, during the period when freely moving larvae experience locomotor impairments (*SI Appendix*, Fig. S1*C*). Moreover, oxygen availability modulated neural activity, the onset of a brain-wide depolarization, and CT_{max}, suggesting that an oxygen- and heat-induced brain dysfunction sets the thermal limit of larvae zebrafish.

DISCUSSION

A massive, heat-induced, seizure-like global depolarization arose in the larval brain at similar temperatures as CT_{max} occurred in freely swimming fish. These brain depolarizations were four to five times the magnitude of medulla locomotor calcium peaks and lasted considerably longer (Fig. 2). This abnormally high neural activity in response to heat stress is reminiscent of heat-induced seizures (31–33) and of heat-induced spreading depolarizations (29), which are slow propagating waves of neuron and glial cells' depolarization (42). The temporal dynamic of the events measured here is characteristic of the latter. First, the depolarizations spread slowly across the brain (Fig. 2*E*) at a speed consistent with that reported for spreading depolarizations [2 to 9 mm/min (42, 43)] and slower than occurs with seizures (44, 45). Second, the long postdepolarization recovery time with lowered neural activity (Fig. 2*D*) is consistent with that seen after spreading depolarizations (42, 46). Overall, the temperatures at which the brain-wide depolarizations occurred, as well as their transient nature, made it a plausible event to explain the reversible unresponsive behavioral state that we observed at CT_{max}.

If upper thermal tolerance in zebrafish larvae is caused by a global depolarization shutting down central nervous system function, the depolarization should coincide with CT_{max} measured in the same individual. Surprisingly, freely swimming larval zebrafish reached CT_{max} before they developed a brain-wide depolarization. This is in contrast with findings of a series of studies on insects in which measures of upper thermal tolerance matched the onset of spreading depolarization in the central nervous system (29, 47). In these studies, upper thermal limits and spreading depolarization onsets were measured in separate individuals—freely moving flies and central nervous system preparations, respectively. Using an approach similar to that in experiments 1 and 2, we also found overlapping temperature ranges for CT_{max} and brain-wide depolarization onset. Only when measuring both parameters simultaneously in the same individuals could we resolve the consistent difference between these consecutive events (Fig. 3*D*) and determine that CT_{max} precedes the depolarization by half a degree, leading us to the conclusion that brain-wide depolarization is not the cause of CT_{max} in larval zebrafish.

As the brain-wide depolarization occurred after CT_{max}, we investigated if neural activity was altered in the period leading

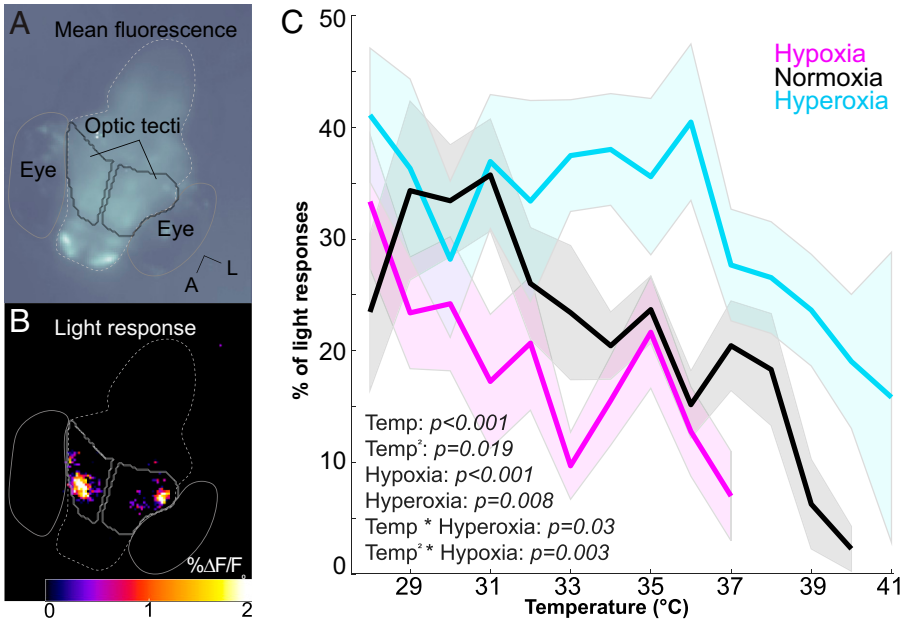

Fig. 6. Oxygen availability affects the sensory-response resilience to heating. (*A*) Mean fluorescence image of the brain (dashed gray line) of an agar-embedded, *Tg(elavl3:GCaMP6s)* 5-d-old fish under an epifluorescence microscope (same setup as in Fig. 5*B*). A, anterior; L, lateral. (*B*) Representative light response to a red-light flash specifically activating the optic tecti in the same fish as in *A*. (*C*) Percentage of responses to light flashes in the optic tectum during heat ramping with water oxygen level of 60% (hypoxia; magenta circles; $n = 14$), 100% (normoxia; black circles; $n = 11$), or 150% (hyperoxia; cyan circles; $n = 13$) of air-saturated water (*Methods*) (*SI Appendix*, Table S10). Temp, temperature.

to the depolarization. We found that neural activity was strongly reduced in locomotor brain regions during the warmest minutes preceding the depolarization (Figs. 2 *F* and 5*D* and *SI Appendix*, Fig. S3*D*). Additionally, the neural responsiveness to light stimuli decreased during heating (Fig. 6*C*). As both the spontaneous brain activity and the brain response to visual stimulation declined toward the upper thermal limit temperatures, we suggest that gradual brain dysfunction, rather than spreading depolarization, is the cause for CT_{max}.

While these results point to progressively deteriorating brain function causing CT_{max}, they are insufficient to determine if the physiological mechanism is through direct thermal effects on neurons or if the impact is mediated by insufficient brain tissue oxygenation. Therefore, we manipulated oxygen water concentrations to test if oxygen availability alters CT_{max} and neural function. We found that hyperoxia (150% air saturation) increased both CT_{max} and neural thermal resilience during heat ramping compared with hypoxia (60%) and normoxia (100%). Neural activity in the locomotor brain center and optic tectum response to visual stimuli were more resilient to high temperature in hyperoxia than in hypoxia and normoxia, demonstrating that the thermal impact on the brain is mediated through tissue oxygenation. Furthermore, similar to the earlier measurements in normoxia, neural activity was largely silenced in the medulla during the very last minutes preceding the brain depolarization, when fish reach their upper thermal limit (Figs. 3*D* and 5*D*). This shows that impairment of the central nervous function coincided with the temperatures where CT_{max} occurs, further suggesting that neural impairment due to lack of oxygen and/or accumulation of anaerobic metabolites contributes to loss of locomotor function observed at the upper thermal limit.

While we focused here on the effect of heat on neurons, glial cells may possibly be a key cellular intermediate in linking oxygen requirements and neural activity at high temperature. Glial cells sense brain oxygen levels (48) and play a crucial role in regulating cerebral blood flow, thereby providing adequate oxygen supply to the brain (49). Moreover, glial cells contribute to intracellular calcium rise in neurons (50), including in conditions where oxygen is lacking (51). Finally, adrenergic modulation of astrocyte activity after cortical spreading depolarization accelerates the recovery of neural activity (52). In future experiments in transgenic zebrafish lines, labeling glial cells (53, 54) will help determine their contribution to heat-induced spreading depolarization.

A few studies have found a positive effect of increased oxygen availability on thermal tolerance. Hyperoxia (200%) improved the upper thermal limit by 1.1 °C in the European perch (55) and by 0.4 °C in the common triplefin (56). Increased aquatic oxygen availability can extend the survival of several ectotherm species (i.e., arthropods, chordates, echinoderms, mollusks, and fish) at extreme temperatures (57, 58). However, hyperoxia did not improve thermal tolerance for a large number of other fish species (25), and only severely hypoxic conditions reduced the upper thermal limit of the red drum and lumpfish (18). Taken together, these studies suggest that oxygen limitation is not a general mechanism limiting thermal tolerance across all species and contexts. Our results emphasize that interspecific differences in neural-tissue resilience to heating and oxygen deprivation, as well as cardiorespiratory capacity, might be critical physiological factors explaining these contrasting results between species and contexts.

Cardiac capacity has been suggested to limit thermal tolerance in fish (59), and to test the resilience of the heart, we measured heart rate during heat ramping. After the expected initial increase in heart rate as temperature increased (22, 60), the heart rate decreased and then it remained stable upon further heating and through the brain depolarization (Fig. 4*C* and *E*). Similarly, a decrease or plateau in heart rate with increasing temperatures has been reported for salmonids (20) and European perch (55). We also measured a simultaneous decrease in heart rate and neural activity (Fig. 4*C* and *SI Appendix*, Fig. S2*B*), which could be explained by shared temperature-induced dysfunctions in excitable cells in the brain and myocardium (14, 61, 62). Brain function appeared less resilient to high temperatures than the

heart, since both spontaneous and sensory-evoked neural activity were completely suppressed near CT_{max}, while the heart kept beating at a maintained rate.

Larval zebrafish mainly rely on cutaneous respiration at 28 °C (63) and it is therefore unclear whether the decline in heart rate at high temperatures would result in significant oxygen limitation to the brain at that life stage. This could be more suitably determined in older fish, in which cardiac limitation could contribute to a mismatch between oxygen delivery and tissue oxygen needs. Such a mismatch may cause developing tissue hypoxia and accumulation of metabolites, which can contribute to a loss of response observed at CT_{max}.

In conclusion, we show that the acute thermal limits of larval zebrafish are not caused by a global brain depolarization but are instead likely caused by a drop in neural activity and responsiveness preceding CT_{max}. In accordance with OCLTT predictions, oxygen availability constrains both brain function and the whole-animal thermal limits during heat ramping.

METHODS

Animals and Housing. Experiments were conducted on 5- to 9-d-old larvae and 7- to 10-mo-old zebrafish (*D. rerio*). Transgenic zebrafish expressing the calcium indicator GCaMP6s in most neurons [*Tg(elavl3:GCaMP6s* (37)] in the *nacre/mitfa* background (64) were used in all experiments. Eggs were collected in the morning and kept at a density of 1/mL in fish water (0.2 g of marine salt and 0.04 L AquaSafe/L carbon-filtrated water). After hatching at 3 dpf, the larvae were kept in small nursery tanks and, after 5 dpf, they were fed twice a day with larval food (Tetramin, Tetra). Fish were maintained under standard laboratory conditions (26.8 ± 0.1 °C; 12/12-h light/dark cycle). All experimental procedures performed on zebrafish were in accordance with the 2010/63/EU directive and approved by the Norwegian Animal Research Authority (Food and Safety Authority permit no. 8578).

Experimental Design. We describe in this article five experiments performed on different fish: measuring CT_{max} in freely swimming zebrafish larvae (experiment 1); recording brain activity during warming in agar-embedded zebrafish larvae (experiment 2); simultaneous recording of CT_{max} and neural events in freely swimming zebrafish larvae (experiment 3); simultaneous recording of heart rate and brain activity during warming in agar-embedded larvae (experiment 4); and recording of CT_{max} and neural function under oxygen manipulation during warming (experiment 5).

Measurement of CT_{max}. CT_{max} measurements were used in experiments 1, 3, and 5. All behavioral experiments were conducted in the afternoon, from 12 PM to 7 PM.

CT_{max} setup. Larval zebrafish swam in the behavioral arena (i.e., the central compartment) of a double-walled, glass heating-mantle made in the glass workshop at the Norwegian University of Science and Technology. The dimensions were as follows: outer diameter, 42 mm; inner diameter, 29 mm; outer height, 32 mm; and inner height, 19 mm. The fish movement was recorded using a webcam (Logitech C270, 720p) positioned above the arena. To enhance contrast, the arena was placed above a background illumination light source. Two outlets connected the glass heating mantle to a water bath. Adjustment of water temperature of the arena was achieved by pumping water from an external heating bath through the heating mantle. The heating rate in the arena was 0.3 °C/min following the protocol described by Morgan et al. (8). The water temperature inside the central chamber of the arena was recorded at 1 Hz using a thermocouple (type K, Pico Technology) connected to a data logger (TC-08, Pico Technology). All temperatures reported refer to that of the fish water inside the arena. The water temperature remained homogeneous within the arena during the heat ramp (the temperature difference between center and periphery was 0.13 ± 0.01 °C), thanks to the constant homogenization via gentle air bubbling and convection.

CT_{max} assay in larval zebrafish. The arena was filled with 3 mL of 28 °C water supplied with air bubbling through a modified hypodermic needle fixed to the side wall of the compartment. At the beginning of a CT_{max} recording, a single larva was carefully transferred to the arena. All individuals were given 15 min to habituate to the arena before the recording started. The CT_{max} assay lasted up to 50 min, during which the temperature within the arena increased from 28 °C by 0.3 °C/min until the larva reached CT_{max}. The temperature was kept constant at 28 °C for recordings of control fish. The fish behavior was recorded at 4 to 7 Hz during four intervals: 28 to 29 °C, 31 to 32 °C, 34 to 35 °C, and 37 °C to CT_{max}. For control larvae, recordings of matching durations were taken at corresponding time points. Methods commonly used to determine CT_{max} in adult fish were unsuitable for 5 dpf larvae zebrafish, since the loss-of-equilibrium criterion (8) also occurred in control fish without heat ramp, and muscular spasms (6) could not be reliably quantified due to the larvae's small size. Thus, CT_{max} was determined as the temperature at which the animal became unresponsive (11, 29, 65), which was defined as the first of three consecutive touches that did not elicit an escape response (loss of response). In both the control and the heat-ramp groups, the stimulations were applied to the larva's trunk throughout the assay, using the tip of a capillary microloader (VWR International). In cases where the fish did not escape a stimulation, a second stimulation was applied after a minimum of 3 s. When a fish failed to respond to three consecutive stimulations (CT_{max}), it was transferred to 28 °C water and visually monitored. Fish that did not recover normal locomotor activity were killed humanely and were not included in the analysis. This happened in 6 of 92 larvae, similar to the mortality rates reported in adult zebrafish in previous studies (8, 66).

CT_{max} assay in adult zebrafish. To compare CT_{max} throughout development, 16 adult *Tg(elavl3:GCaMP6s)* zebrafish, aged 7 to 10 mo, were tested in the CT_{max} setup described by Morgan et al. (8). The fish were tested in groups of eight fish in a rectangular acrylic tank (25-cm long, 20-cm wide, 18-cm deep) filled with 9 L of water. Individual CT_{max} was measured at the temperature of loss of equilibrium determined as 2 s of inability to maintain postural stability (8). The fish were removed immediately after the criterion was reached. All animals survived the test.

CT_{max} assay data analysis. The fish position was manually detected in MATLAB (MathWorks 2018) at the temperature ranges 28 to 29 °C, 31 to 32 °C, 34 to 35 °C, and 37 to 38 °C and during the 1 °C increase preceding CT_{max}. The average speed was calculated during these intervals. Loss of equilibrium and spiral swimming events were manually labeled by an experimenter during the 12 min preceding CT_{max} in heat ramp fish and during the corresponding period in control fish. Loss of equilibrium was recorded when the fish tilted to the side for at least 1 s (Movie S2). A spiral swimming event was recorded when the fish rapidly swam in a minimum of two consecutive circles with diameter less than 5 mm (Movie S1).

Brain Activity during Warming in Agar-Embedded Larvae. For the imaging of neural activity in embedded fish in experiments 2, 4, and 5, a 5-d-old larva was embedded at the bottom of the central glass compartment in 2% low-gelling-temperature agarose (Merck). The agarose was carefully removed around the eyes and mouth upon hardening and the arena was filled with 3 mL of water. Calcium fluorescence was recorded with a custom-made epifluorescence microscope equipped with a ×10 water-immersion objective (UMPLFLN, Olympus), a set of green fluorescent protein emission-excitation filters (FGL400, MD498, and MF525-9, Thorlabs) and a mounted blue light-emitting diode (LED) controlled by a driver (MWWHL4, LEDD1B, Thorlabs). Images were collected at 5 Hz via a custom-written Python script using the Pymba wrapper for interfacing with the camera (Mako G319B, Allied Vision).

Simultaneous Recording of CT_{max} and Depolarization in Freely Swimming Larvae. In experiment 3, calcium imaging in freely swimming fish was used to record CT_{max} and brain-wide depolarization simultaneously in the same individuals. The double-walled glass heating-mantle was placed under an epifluorescence microscope (AxioImager, ZEISS) equipped with a megapixel camera (AxioCam 506, ZEISS) and Plan-NEOFLUAR 2 ×1 objective. The larva was swimming at the center of the arena, within a 13-mm diameter region delimited with a nylon mesh, to match the limited field of view of the microscope (14 × 14 mm). Time lapse of fluorescent images was recorded at 5 Hz using the Zen software (ZEN Lite Blue, ZEISS). Since the recordings were made in the dark, the experimenter watched the live recording display of the recording on the computer screen to visually guide the pokes to the fish trunk. The nylon mesh created a small thermal gradient in the arena from the central part to the outer

area outside the mesh. During the experimental trials, the temperature was recorded outside the mesh to ensure a full view of the fish. The temperature gradient was quantified in an additional experiment over six heat ramps by recording the temperature in the arena center and outside the mesh near the outer wall of the arena with two thermocouples at each location. The gradient was accounted for to calculate the water temperature the fish was exposed to.

Cardiac Function and Brain Activity during Heat Ramping in Agar-Embedded Larvae. In experiment 4, heart rate and neural activity were simultaneously recorded at 20 Hz in laterally mounted larvae under an epifluorescence microscope (AxioImager, ZEISS) equipped with a megapixel camera (AxioCam 506, ZEISS). Recordings were corrected for drift when needed using Fiji's Template matching plugin. Whole brain and heart regions of interest were selected in Fiji. Fish whose heart was out of focus during more than two recording intervals ($n = 1$ of 10 fish) and frames where movement artifacts could not be corrected were not included. Heartbeat frequency during a recording interval was calculated using MATLAB's continuous wavelet transform function (*cwt*).

Oxygen Effects on CT_{max} and Neural Function during Warming. Due to problems with data storage causing the loss of five recordings of neural activity in the initial data collection in July 2020, we set up an additional round of assays for experiment 5 in January 2021. The effect of the experimental period was tested for in the statistical analyses (*Statistical analyses*).

CT_{max} assay with oxygen-level manipulation. The same CT_{max} setup described for experiment 1 was used to record the effect of oxygen manipulation on CT_{max} in experiment 5. The arena was intermittently bubbled with pure oxygen or pure nitrogen to increase or decrease oxygen levels, respectively. The bubbling flow rate was manually adjusted using tubing clamps. A fiber-optic oxygen probe (OXROB10, Pyro Science) and a temperature probe (TSUB21, Pyro Science) connected to an oxygen and temperature meter (FireSting-O2, Pyro Science) were placed in the chamber to monitor and record the oxygen levels during the assay. The oxygen saturation level was displayed in real time using oxygen logger software (Pyro oxygen logger, Pyro Science) and kept at 150% or 60% of air saturation during the whole CT_{max} assay by manually adjusting the bubbling intensity.

Recording neural activity with oxygen-level manipulation. The same epifluorescence calcium imaging setup described for experiment 2 was used to measure neural activity during heat ramping with oxygen manipulation. For the control treatment, the water was bubbled with air through a modified hypodermic needle and maintained at 100% oxygen of air saturation during the trials. To decrease oxygen saturation, the water was bubbled with nitrogen, and to increase the oxygen level, oxygen was gently blown on the surface. A bare fiber microsensor (OXB430, Pyro Science) and a temperature probe (TDIP15, Pyro Science) were placed in the chamber to monitor and record oxygen levels. Oxygen levels were manually adjusted to either 150% or 60% of air-saturated water for the high and low oxygen treatments, respectively. Additionally, the larvae were visually stimulated using pulses of light (2 s long, every 30 s) using a red LED equipped with a laser line filter (FL05635-10, central wavelength 635 nm, Thorlabs) positioned in front of the fish. The LED was connected to an Arduino board (Arduino mini) and synchronized with the camera using custom-written Python scripts.

Calcium-Imaging Data Analyses.

In agar-embedded fish. Calcium imaging recordings were corrected for slow drift due to agarose expansion using the Fiji's (67) template-matching plugin (*Align slices in stack*). The regions of interest corresponding to the whole brain, the telencephalon, the optic tectum, and the medulla were manually segmented.

The raw calcium fluorescence signal was calculated by averaging all pixels within a region. To reproducibly detect the brain-wide depolarization onset time across fish, the whole-brain raw fluorescence signal was first processed to filter out the calcium events using a second order Butterworth filter (low pass, 0.01-Hz cutoff frequency). The average value and SD of the filtered trace's time derivative were calculated during the 17 min preceding the approximate onset of the depolarization. The depolarization onset was set when the time derivative exceeded the average baseline value by more than 5 SDs.

For calcium peak detection, the fluorescence change was calculated in the left and right medulla using a sliding window of the previous 2 min. Fish in which the signal was weak and noisy due to uneven mounting were not included in the analysis. The calcium peaks were detected automatically using the MATLAB function *findpeaks* and calcium peak frequency (peaks/min) was then averaged across both medullae. For calculation of calcium peaks frequency in laterally embedded fish during shorter recordings (*SI Appendix*, Fig. S2*B*), the raw fluorescence was measured in the medulla, and calcium peaks were visually detected.

The peak depolarization amplitude (*SI Appendix*, Fig. S3*B*) was determined as the maximum returned by the *findpeaks* function after depolarization onset. The recovery time (*SI Appendix*, Fig. S3*C*) was the duration between peak depolarization and the return to baseline value (0%$\Delta F/F_0$), with $\%\Delta F/F0 = (Ft - F_0)/F_0 \times 100$, where F_0 is the averaged fluorescence during the 5 min before the depolarization onset and Ft the fluorescence at time t. One fish from the hyperoxic treatment was not included as the recordings ended before the fluorescence reached baseline after the depolarization.

For light responses (Fig. 6 and *SI Appendix*, Fig. S4), the percentage change in fluorescence in the optic tecti was calculated as $\%\Delta F/F_0 = (F_t - F_0)/F_0 \times 100$, where F_0 is the averaged fluorescence during the 2 s before a stimulus and F_t the fluorescence at time t. The amplitude of the light response was then calculated by averaging the $\%\Delta F/F_0$ during the 4 s after the stimulus onset. To account for the interindividual variation in fluorescence, optic tectum responses were calculated as binary outcomes. The optic tecti were categorized responsive (*response*) if the light response amplitude exceeded 2 SDs above F_0, and otherwise were categorized as not responsive (*no response*).

In freely moving fish. Measuring brain-wide fluorescence during the freely swimming assay in experiment 2 was cumbersome due to the fish moving and tilting. Thus, the depolarization-onset temperature was determined by two investigators who independently selected the time at which the fluorescence increased abruptly in the brain. The final depolarization-onset value was obtained by averaging both estimates (agreement between experimenters was, on average, within 19 ± 4 s out of 55 min).

Statistical Analyses. Data are reported as mean and SEM. All statistical analyses were conducted in R, version 4.1.1 (68). We used ANOVAs on independent measurements, and the assumptions of normality and homoscedasticity of residual variance were assessed visually using residual plots. Alternative models were considered if assumptions were violated. For responses recorded as repeated measures on individual fish, mixed models were created using the *lmer* function from the *lme4* package, v.1.1–27.1, to account for fish identity as a random effect. Data for experiment 5 were collected over two sampling periods and experiment (1 or 2) was included as a fixed factor in the models to test the effect of this. Akaike information criterion was used to consider interactions in models with two or more predictor variables. Models are also presented with and without data points that were considered extreme outliers ($<Q1 - 3 \times$ interquartile range or $>Q3 + 3 \times$ interquartile range). Summaries of all models are presented in *SI Appendix*, Tables S1 through S10 with effect size of predictor variables (β), their SE, t and P values estimated by the respective models, and the R^2 for the fixed effects. The significance of effects was considered with a P value criterion of $P < 0.05$. For a detailed description of statistical analyses of all models, see *SI Appendix*, *SI Statistical Analyses*.

Data, Materials, and Software Availability. All datasets from this study and R code for the statistical analyses and figures have been deposited in figshare (https://doi.org/10.6084/m9.figshare.19640805) (69).

ACKNOWLEDGMENTS. The authors thank Florian Engert and Alex Shier for sharing the *Tg(elavl3:GCaMP6s)* line, Eline Rypdal for fish care, the members of the Animal Physiology section at the Department of Biology for scientific discussions, and Marius Maehlum for the heartbeat-frequency analysis code. The authors also thank Johannes Overgaard and an anonymous reviewer for their constructive feedback on earlier drafts of this manuscript.

Funding. This work was supported by the Research Council of Norway (funding scheme for independent projects [FRIPRO] grants FK: 262698 and FJ: 262942).

1. S. I. Seneviratne, M. G. Donat, B. Mueller, L. V. Alexander, No pause in the increase of hot temperature extremes. *Nat. Clim. Chang.* **4**, 161–163 (2014).
2. J. H. Stillman, Heat waves, the new normal: Summertime temperature extremes will impact animals, ecosystems, and human communities. *Physiology (Bethesda)* **34**, 86–100 (2019).
3. C. A. Deutsch *et al.*, Impacts of climate warming on terrestrial ectotherms across latitude. *Proc. Natl. Acad. Sci. U.S.A.* **105**, 6668–6672 (2008).
4. P. M. Schulte, The effects of temperature on aerobic metabolism: Towards a mechanistic understanding of the responses of ectotherms to a changing environment. *J. Exp. Biol.* **218**, 1856–1866 (2015).
5. M. L. Pinsky, A. M. Eikeset, D. J. McCauley, J. L. Payne, J. M. Sunday, Greater vulnerability to warming of marine versus terrestrial ectotherms. *Nature* **569**, 108–111 (2019).
6. W. I. Lutterschmidt, V. H. Hutchison, The critical thermal maximum: History and critique. *Can. J. Zool.* **75**, 1561–1574 (1997).
7. C. D. Becker, R. G. Genoway, Evaluation of the critical thermal maximum for determining thermal tolerance of freshwater fish. *Environ. Biol. Fishes* **4**, 245 (1979).
8. R. Morgan, M. H. Finnøen, F. Jutfelt, CT_{max} is repeatable and doesn't reduce growth in zebrafish. *Sci. Rep.* **8**, 7099 (2018).
9. J. M. Sunday, A. E. Bates, N. K. Dulvy, Thermal tolerance and the global redistribution of animals. *Nat. Clim. Chang.* **2**, 686–690 (2012).
10. A. Genin, L. Levy, G. Sharon, D. E. Raitsos, A. Diamant, Rapid onsets of warming events trigger mass mortality of coral reef fish. *Proc. Natl. Acad. Sci. U.S.A.* **117**, 25378–25385 (2020).
11. M. J. Friedlander, N. Kotchabhakdi, C. L. Prosser, Effects of cold and heat on behavior and cerebellar function in goldfish. *J. Comp. Physiol.* **112**, 19–45 (1976).
12. F. Jutfelt *et al.*, Brain cooling marginally increases acute upper thermal tolerance in Atlantic cod. *J. Exp. Biol.* **222**, jeb208249 (2019).
13. H. O. Pörtner, C. Bock, F. C. Mark, Oxygen- and capacity-limited thermal tolerance: Bridging ecology and physiology. *J. Exp. Biol.* **220**, 2685–2696 (2017).
14. M. Vornanen, Feeling the heat: Source-sink mismatch as a mechanism underlying the failure of thermal tolerance. *J. Exp. Biol.* **223**, jeb225680 (2020).
15. F. E. J. Fry, *Effects of the Environment on Animal Activity* (University of Toronto Press, 1947).
16. H. O. Pörtner, R. Knust, Climate change affects marine fishes through the oxygen limitation of thermal tolerance. *Science* **315**, 95–97 (2007).
17. R. Ern, A mechanistic oxygen- and temperature-limited metabolic niche framework. *Philos. Trans. R. Soc. Lond. B Biol. Sci.* **374**, 20180540 (2019).
18. R. Ern, T. Norin, A. K. Gamperl, A. J. Esbaugh, Oxygen dependence of upper thermal limits in fishes. *J. Exp. Biol.* **219**, 3376–3383 (2016).
19. H. O. Pörtner, Climate variations and the physiological basis of temperature dependent biogeography: Systemic to molecular hierarchy of thermal tolerance in animals. *Comp. Biochem. Physiol. A Mol. Integr. Physiol.* **132**, 739–761 (2002).
20. A. P. Farrell, Environment, antecedents and climate change: Lessons from the study of temperature physiology and river migration of salmonids. *J. Exp. Biol.* **212**, 3771–3780 (2009).
21. R. Ern, T. T. Huong, N. T. Phuong, T. Wang, M. Bayley, Oxygen delivery does not limit thermal tolerance in a tropical eurythermal crustacean. *J. Exp. Biol.* **217**, 809–814 (2014).
22. A. P. Farrell, Cardiorespiratory performance during prolonged swimming tests with salmonids: A perspective on temperature effects and potential analytical pitfalls. *Philos. Trans. R. Soc. Lond. B Biol. Sci.* **362**, 2017–2030 (2007).
23. R. Ern *et al.*, Some like it hot: Thermal tolerance and oxygen supply capacity in two eurythermal crustaceans. *Sci. Rep.* **5**, 10743 (2015).
24. W. C. E. P. Verberk *et al.*, Does oxygen limit thermal tolerance in arthropods? A critical review of current evidence. *Comp. Biochem. Physiol. A Mol. Integr. Physiol.* **192**, 64–78 (2016).
25. T. J. McArley, E. Sandblom, N. A. Herbert, Fish and hyperoxia–From cardiorespiratory and biochemical adjustments to aquaculture and ecophysiology implications. *Fish Fish.* **22**, 324–355 (2021).
26. F. Jutfelt *et al.*, Oxygen- and capacity-limited thermal tolerance: Blurring ecology and physiology. *J. Exp. Biol.* **221**, jeb169615 (2018).
27. S. Lefevre, Are global warming and ocean acidification conspiring against marine ectotherms? A meta-analysis of the respiratory effects of elevated temperature, high CO_2 and their interaction. *Conserv. Physiol.* **4**, cow009 (2016).
28. J. R. Brett, Some principles in the thermal requirements of fishes. *Q. Rev. Biol.* **31**, 75–87 (1956).
29. L. B. Jørgensen, R. M. Robertson, J. Overgaard, Neural dysfunction correlates with heat coma and CT_{max} in *Drosophila* but does not set the boundaries for heat stress survival. *J. Exp. Biol.* **223**, jeb218750 (2020).
30. E. Marder, S. A. Haddad, M. L. Goeritz, P. Rosenbaum, T. Kispersky, How can motor systems retain performance over a wide temperature range? Lessons from the crustacean stomatogastric nervous system. *J. Comp. Physiol. A Neuroethol. Sens. Neural Behav. Physiol.* **201**, 851–856 (2015).
31. C. Dube *et al.*, Prolonged febrile seizures in the immature rat model enhance hippocampal excitability long term. *Ann. Neurol.* **47**, 336–344 (2000).
32. S. Shinnar, T. A. Glauser, Febrile seizures. *J. Child Neurol.* **17** (suppl. 1), S44–S52 (2002).
33. R. F. Hunt, G. A. Hortopan, A. Gillespie, S. C. Baraban, A novel zebrafish model of hyperthermia-induced seizures reveals a role for $TRPV_4$ channels and NMDA-type glutamate receptors. *Exp. Neurol.* **237**, 199–206 (2012).
34. T. D. Clark, E. Sandblom, F. Jutfelt, Aerobic scope measurements of fishes in an era of climate change: Respirometry, relevance and recommendations. *J. Exp. Biol.* **216**, 2771–2782 (2013).
35. T. D. Clark, E. Sandblom, F. Jutfelt, Response to Farrell and to Portner and Giomi. *J. Exp. Biol.* **216**, 4495–4497 (2013).
36. F. Jutfelt *et al.*, Response to 'How and how not to investigate the oxygen and capacity limitation of thermal tolerance (OCLTT) and aerobic scope–Remarks on the article by Gräns et al. *J. Exp. Biol.* **217**, 4433–4435 (2014).
37. N. Vladimirov *et al.*, Light-sheet functional imaging in fictively behaving zebrafish. *Nat. Methods* **11**, 883–884 (2014).
38. R. M. Robertson, T. G. Money, Temperature and neuronal circuit function: Compensation, tuning and tolerance. *Curr. Opin. Neurobiol.* **22**, 724–734 (2012).
39. L. S. Tang, A. L. Taylor, A. Rinberg, E. Marder, Robustness of a rhythmic circuit to short- and long-term temperature changes. *J. Neurosci.* **32**, 10075–10085 (2012).
40. L. Turrini *et al.*, Optical mapping of neuronal activity during seizures in zebrafish. *Sci. Rep.* **7**, 3025 (2017).
41. M. B. Ahrens, K.-H. Huang, S. Narayan, B. D. Mensh, F. Engert, Two-photon calcium imaging during fictive navigation in virtual environments. *Front. Neural Circuits* **7**, 104 (2013).
42. K. E. Spong, R. D. Andrew, R. M. Robertson, Mechanisms of spreading depolarization in vertebrate and insect central nervous systems. *J. Neurophysiol.* **116**, 1117–1127 (2016).
43. J. Woitzik *et al.*; COSBID study group, Propagation of cortical spreading depolarization in the human cortex after malignant stroke. *Neurology* **80**, 1095–1102 (2013).
44. M. Wenzel, J. P. Hamm, D. S. Peterka, R. Yuste, Reliable and elastic propagation of cortical seizures in vivo. *Cell Rep.* **19**, 2681–2693 (2017).
45. J. Liu, S. C. Baraban, Network properties revealed during multi-scale calcium imaging of seizure activity in zebrafish. *eneuro* **6**, ENEURO.0041-19.2019 (2019).
46. P. M. Sawant-Pokam, P. Suryavanshi, J. M. Mendez, F. E. Dudek, K. C. Brennan, Mechanisms of neuronal silencing after cortical spreading depression. *Cereb. Cortex* **27**, 1311–1325 (2017).
47. M. K. Andersen, N. J. S. Jensen, R. M. Robertson, J. Overgaard, Central nervous system shutdown underlies acute cold tolerance in tropical and temperate *Drosophila* species. *J. Exp. Biol.* **221**, jeb179598 (2018).
48. P. R. Angelova *et al.*, Functional oxygen sensitivity of astrocytes. *J. Neurosci.* **35**, 10460–10473 (2015).
49. D. Attwell *et al.*, Glial and neuronal control of brain blood flow. *Nature* **468**, 232–243 (2010).
50. C. Diaz Verdugo *et al.*, Glia-neuron interactions underlie state transitions to generalized seizures. *Nat. Commun.* **10**, 3830 (2019).
51. R. Helleringer, O. Chever, H. Daniel, M. Galante, Oxygen and glucose deprivation induces Bergmann glia membrane depolarization and Ca^{2+} rises mainly mediated by K^+ and ATP increases in the extracellular space. *Front. Cell. Neurosci.* **11**, 349 (2017).
52. H. Monai *et al.*, Adrenergic inhibition facilitates normalization of extracellular potassium after cortical spreading depolarization. *Sci. Rep.* **11**, 8150 (2021).
53. J. Chen, K. E. Poskanzer, M. R. Freeman, K. R. Monk, Live-imaging of astrocyte morphogenesis and function in zebrafish neural circuits. *Nat. Neurosci.* **23**, 1297–1306 (2020).
54. Y. Mu *et al.*, Glia accumulate evidence that actions are futile and suppress unsuccessful behavior. *Cell* **178**, 27–43.e19 (2019).
55. A. Ekström *et al.*, Cardiac oxygen limitation during an acute thermal challenge in the European perch: Effects of chronic environmental warming and experimental hyperoxia. *Am. J. Physiol. Regul. Integr. Comp. Physiol.* **311**, R440–R449 (2016).
56. T. J. McArley, A. J. R. Hickey, N. A. Herbert, Hyperoxia increases maximum oxygen consumption and aerobic scope of intertidal fish facing acutely high temperatures. *J. Exp. Biol.* **221**, jeb189993 (2018).
57. W. C. E. P. Verberk, R. S. E. W. Leuven, G. van der Velde, F. Gabel, Thermal limits in native and alien freshwater peracarid Crustacea: The role of habitat use and oxygen limitation. *Funct. Ecol.* **32**, 926–936 (2018).
58. F. Giomi *et al.*, Oxygen supersaturation protects coastal marine fauna from ocean warming. *Sci. Adv.* **5**, eaax1814 (2019).
59. A. P. Farrell, Cardiorespiratory performance in salmonids during exercise at high temperature: Insights into cardiovascular design limitations in fishes. *Comp. Biochem. Physiol. A Mol. Integr. Physiol.* **132**, 797–810 (2002).
60. M. J. Gollock, S. Currie, L. H. Petersen, A. K. Gamperl, Cardiovascular and haematological responses of Atlantic cod (*Gadus morhua*) to acute temperature increase. *J. Exp. Biol.* **209**, 2961–2970 (2006).
61. S. Buzatu, The temperature-induced changes in membrane potential. *Riv. Biol.* **102**, 199–217 (2009).
62. M. Vornanen, The temperature dependence of electrical excitability in fish hearts. *J. Exp. Biol.* **219**, 1941–1952 (2016).
63. P. Rombough, Gills are needed for ionoregulation before they are needed for $O(_2)$ uptake in developing zebrafish, *Danio rerio*. *J. Exp. Biol.* **205**, 1787–1794 (2002).
64. J. A. Lister, C. P. Robertson, T. Lepage, S. L. Johnson, D. W. Raible, Nacre encodes a zebrafish microphthalmia-related protein that regulates neural-crest-derived pigment cell fate. *Development* **126**, 3757–3767 (1999).
65. E. Sherman, D. Levitis, Heat hardening as a function of developmental stage in larval and juvenile *Bufo americanus* and *Xenopus laevis*. *J. Therm. Biol.* **28**, 373–380 (2003).
66. E. R. Åsheim, A. H. Andreassen, R. Morgan, F. Jutfelt, Rapid-warming tolerance correlates with tolerance to slow warming but not growth at non-optimal temperatures in zebrafish. *J. Exp. Biol.*, **223**, jeb229195 (2020).
67. J. Schindelin *et al.*, Fiji: An open-source platform for biological-image analysis. *Nat. Methods* **9**, 676–682 (2012).
68. R Core Team, *R: A Language and Environment for Statistical Computing* (R Foundation for Statistical Computing, 2021).
69. A. Andreassen, P. Hall, P. Khatibzadeh, F. Jutfelt, F. Kermen, R script and datasets for statistical analyses and graphs. figshare. https://figshare.com/articles/software/R_script_for_statistical_analyses_and_graphs/19640805. Deposited 1 September 2022.